**Superalloys 2004**
*Edited by K.A. Green, T.M. Pollock, H. Harada,*
*T.E. Howson, R.C. Reed, J.J. Schirra, and S. Walston*
***TMS (The Minerals, Metals & Materials Society), 2004***

# NEW PHASES IN RUTHENIUM-CONTAINING SINGLE-CRYSTAL SUPERALLOYS

Q. Feng[1], T. K. Nandy[1, 2], L. J. Rowland[1], B. Tryon[1], D. Banerjee[2] and T. M. Pollock[1]
[1]Department of Materials Science and Engineering, University of Michigan, Ann Arbor, MI 48109, USA
[2]Defense Metallurgical Research Laboratory, Hyderabad-500 258, India

Keywords: Nickel alloys, Ruthenium, Rhenium, Intermetallic compounds, Microstructure

## Abstract

Phases present in a series of model ruthenium containing Ni-base single crystal superalloys were investigated in both as-solidified and heat-treated crystals. Three unusual Ru-rich phases have been identified including a $L2_1$ Heusler phase with a composition of $Ru_2AlTa$, a B2 RuAl phase and a hcp Re(Ru)-rich phase. These phases have been characterized in terms of the microstructure, composition, crystallography, three-dimensional morphology and distribution within the dendritic microstructure via X-ray, SEM and TEM analyses.

## Introduction

As a result of progress in both alloy development and casting technology, the temperature capabilities of high-pressure turbine blades have increased by 125°C in the past three decades, resulting in three generations of commercial single crystal alloys [1]. Development of successive generations of single crystal superalloys has been driven by the need for continuous increases in the performance and efficiency of aircraft and power generation turbines.

To design alloys with long term microstructural stability at high temperatures requires a detailed knowledge of phase equilibria in multicomponent Ni-base alloy systems. Ni-based superalloys contain at least two basic phases, a disordered fcc γ matrix and ordered $L1_2$ γ' precipitates based on $Ni_3Al$. In addition to these phases, a large number of secondary phases may be present including carbides, borides and numerous ordered intermetallic phases, with the most notable being the deleterious topologically-close-packed (TCP) phases.

"Fourth generation" single crystal alloys with ruthenium as a new alloying addition have recently been under development [2, 3]. Ruthenium is one of the four elements along with tungsten, rhenium and iridium that increase the liquidus and solidus temperatures of nickel [4]. Ru additions to multicomponent Ni-base superalloys also increase liquidus temperatures [5], suggesting that Ru additions are promising in terms of improving the temperature capabilities of these materials. Ru additions to Ni-base superalloys have been reported to influence the partitioning behavior of the constituent elements to the γ and γ' phases, increase the microstructural stability at high temperatures and lower the propensity for TCP phase formation and thus improve stress rupture life [2]. However, there have been limited systematic studies on Ru-containing Ni-base superalloys, particularly with respect to the fundamentals of phase equilibria and microstructural stability in these new, complex alloy systems.

With ruthenium additions to Ni-base superalloys, new secondary phases might be expected to precipitate during solidification or in subsequent thermal exposures. This paper reports new Ru-rich phases in multicomponent Ru-containing Ni-base superalloys in both as-cast and heat-treated conditions. This paper also presents detailed characterization studies of these phases, including their morphology, composition and distribution within the dendritic microstructure. New phases were identified using electron diffraction and X-ray diffraction analyses.

## Experimental Procedures

A series of about thirty multicomponent Ru-containing Ni-base superalloys with variable levels of alloying additions were designed as part of an experimental program to investigate phase equilibria, creep properties and long term microstructural stability at high temperature exposures. The systematic compositional variations of the constituents in these alloys are listed in Table 1. The present investigation differs from previous studies [2, 3, 6] in that a much broader and higher range of Ru additions (2.5-9at.%/4.1-14.1 wt.%) have been studied.

The designed alloys were initially vacuum induction melted (VIM) at Sophisticated Alloys, Inc. and cast into 75 mm diameter cylindrical ingots as polycrystalline materials weighing ~2.5 kg each. The as-cast microstructure in a cylindrical slice sectioned in the middle of each ingot was initially characterized. Following this, solidus and liquidus temperatures and other phase transformations in the as-cast polycrystalline alloys were investigated in a SETERAM SETSYS 18 Differential Thermal Analysis (DTA) instrument. DTA procedures have been described in more detail in a previous paper [5]. Based on DTA results and microstructural evaluations, selected alloys were directionally solidified (DS) into cylindrical bars with ceramic cluster molds in a 50kW ALD Bridgman furnace with a withdrawal rate of 200 mm/h. Prior to withdrawal, the charge ingots were vacuum induction melted and poured into the investment molds preheated to 1550°C. Conventional helical starters were utilized to initiate single crystal growth. Heat treatment experiments of VIM alloys and DS alloys were conducted in an air atmosphere. The investigated alloys were subjected to a solution treatment of 1300-1320°C for 4-12 hours, with subsequent water quenching or air cooling, and aging at 950-1150°C for 20-1500 hours. Initial microstructural observations on as-cast and heat-treated crystals were conducted with an optical microscope and a Philips/FEI XL30FEG scanning electron microscope (SEM) operated in secondary electron (SE) and back-scattered electron (BSE) imaging modes. Semi-quantitative chemical analyses were

Table 1. The composition range of the investigated multicomponent Ru-containing Ni-base superalloys.

| | Al | Co | Cr | Re | Ru | Ta | W | Ni |
|---|---|---|---|---|---|---|---|---|
| Atomic percent | 13.3 – 18.4 | 2.4 – 10.1 | 0 – 8.0 | 1.3 – 2.5 | 2.5 – 9.0 | 2.3 – 3.3 | 1.0 – 4.5 | Balance |
| Weight percent | 5.6 – 8.1 | 2.5 – 10.5 | 0 – 6.9 | 3.6 – 7.5 | 4.1 – 14.1 | 6.1 – 9.9 | 2.9 – 12.4 | Balance |

performed with a standardless energy dispersive spectrometer (EDS) attached to the SEM or TEM. Quantitative analyses were obtained using a Cameca CAMEBAX or a SX-100 electron microprobe, calibrated from the standards of pure elements, except Al for which an alloy of Ni-30wt.% Al was used.

For as-cast and heat-treated alloys in which the additional phases besides the γ and γ' phases were observed, electrolytic extraction experiments were performed to obtain concentrated quantities of the additional phases. In the electrolytic extraction process, the bulk sample (anode) was immersed into a solution of 9:1 Methanol:HCl + 1 wt.% tartaric acid for 6 hours to dissolve the γ and γ' phases with a platinum sheet used as a cathode. Subsequently, the residue was collected, dried and investigated by a Rigaku X-ray Diffractometer (XRD) equipped with a Cu target. The measurements were carried out for 2θ values from 20 to 120 degrees at a scanning rate of $1^o$/min. Phase morphologies of partially extracted precipitates were examined by SEM. Transmission electron microscopy (TEM) was also utilized for phase identification in a JEOL 4000 or a Philips CM12 electron microscope at the accelerating voltage of 400 kV and 120 kV, respectively. The TEM specimens were prepared by twin-jet electro-polishing or ion milling techniques since the precipitates contained high levels of refractory alloying additions (Ru, Re and Ta) and could not be thinned simultaneously with the γ and γ' phases by jet polishing. The pre-dimpled specimens were ion-milled in a Gatan 691 Precision Ion Polishing System (PIPS™). Operating conditions included a 6-$8^o$ inclination angle and 3.5-4.0 kV acceleration voltages.

## Results

Microstructural investigations were conducted on a set of thirty multicomponent Ni-base superalloys containing ruthenium. The compositional range of these alloys, designated as the UM-F series, is summarized in Table 1. A number of these alloys contained significant amounts of unusual Ru-rich phases in as-cast or heat-treated conditions. The nominal compositions of the alloys containing these phases are listed in Table 2 along with the composition of the baseline alloy UM-F9. It is interesting to note that alloy UM-F16 is the only alloy containing chromium. For the comparative purposes, the nominal composition of each alloy is also listed in Tables 4-6 along with the chemical analyses of Ru-rich phases. Three new phases are reported separately in the following three sections, although they may co-exist in a single alloy. The basic crystallography of these phases is first summarized in Table 3 and Figure 1. Additional details on the characteristics of each phase (morphology, composition, lattice parameters and orientation relationship) are presented.

Table 2. Nominal compositions of the investigated alloys (at.%).

| Materials | Al | Co | Cr | Re | Ru | Ta | W | Ni |
|---|---|---|---|---|---|---|---|---|
| UM-F3 | 18.4 | 7.5 | - | 1.8 | 2.5 | 2.5 | 1.5 | 65.8 |
| UM-F9 | 14.3 | 7.5 | - | 1.3 | 6.0 | 2.3 | 1.5 | 67.1 |
| UM-F13 | 13.3 | 7.5 | - | 1.3 | 9.0 | 2.3 | 1.5 | 65.1 |
| UM-F14 | 14.3 | 7.5 | - | 2.5 | 6.0 | 2.3 | 1.5 | 65.9 |
| UM-F16 | 14.3 | 7.5 | 8.0 | 1.3 | 6.0 | 2.3 | 1.5 | 59.1 |

### The $L2_1$ Heusler (H) phase $Ru_2AlTa$

The $L2_1$ Heusler phase $Ru_2AlTa$ was first observed in an aged Ni-base superalloy, UM-F13, which contains very high levels of ruthenium (9.0 at.%/14.1 wt.%).

A typical dendritic microstructure was found in the as-solidified alloy UM-F13. No additional phases beyond the γ and/or γ' phases were observed in the as-solidified or solution-treated microstructure. The γ' phase and the eutectic pools were completely dissolved into the γ matrix after a solution treatment of $1300^o$C/4h. Figure 2(a) is a BSE image of the typical aged microstructure of DS alloy UM-F13, sectioned normal to the <001> growth direction after an aging treatment at $1100^o$C/100h. It clearly shows: (1) residual chemical inhomogeneity within the dendritic microstructure; (2) segregation of heavy elements is within the dendrite cores; and (3) brightly-contrasting precipitates (subsequently identified as the H phase) located in both dendritic and interdendritic regions. Figure 2(b) is a higher magnification BSE image of the framed area in Figure 2(a). It clearly demonstrates a microstructure consisting of γ matrix (gray), γ' precipitates (dark) and H precipitates (white), with the H precipitates primarily enveloped by the γ matrix. The H precipitates were preferentially oriented in the microstructure, indicating a strong orientation relationship between the H precipitates and [010]/[100] secondary dendrite-growth directions. The three-dimensional morphology of H precipitates remaining in an electrolytically extracted bulk sample is shown in Figure 2(c). The H precipitates have a distinctive faceted rod-like morphology. The average composition of larger extracted H precipitates measured by microprobe analysis is listed in Table 4. The H precipitates were strongly enriched in Ru, Ta and Al, but strongly depleted in Re. Interestingly, for the precipitates examined, the H

Table 3. Basic crystallography of Heusler (H), B2 and δ phases.

| Phase | Basic structure | Prototype | Strukturbericht symbol | Pearson symbol | Space group | Space group number | Lattice parameter |
|---|---|---|---|---|---|---|---|
| Heusler | Ordered bcc | $Cu_2AlMn$ | $L2_1$ | cF16 | $Fm\bar{3}m$ | 225 | a= 0.609-0.615 |
| B2 | Ordered bcc | CsCl | B2 | cP2 | $Pm\bar{3}m$ | 221 | a= 0.299-0.304 |
| δ | Hexagonal | Mg | A3 | hP2 | $P6_{3/mmc}$ | 194 | a=0.270-0.271<br>c=0.431-0.435 |

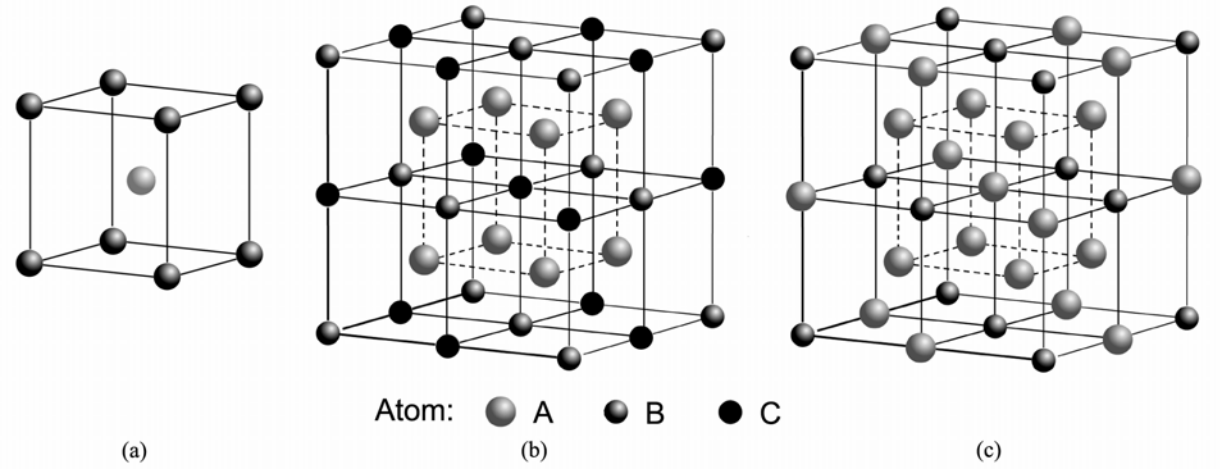


Figure 1. Ordered bcc-derivated crystal lattices, (a) B2, (b) $L2_1$ and (c) $D0_3$

phase contained Ru as high as 45 at. %, which is almost equal to the total atomic percentage of (Al + Ta). In order to understand the distribution of the H precipitates, the average compositions of dendrite cores and interdendritic regions as well as eutectic regions in the as-solidified alloy UM-F13 were also measured by a microprobe and are given in Table 4. It was found that Ru preferentially partitioned to the dendrite core, but with much less pronounced segregation compared to Re and W. The Ta and Al segregated to the interdendritic regions with very strong partitioning of Ta to the γ+γ' eutectic pools.

Since there is no Ru-Al-Ta ternary equilibrium phase diagram available, the existence of ternary phases in this system has not yet been explored in any detail. Thus, a range of techniques were required for the identification of this previously undiscovered Ru-rich H phase. Ru-rich B2 phases are known to exist in the Ru-Al and Ru-Ta binary systems [4] as well as in the Ni-Al-Ru ternary system [7]. Crystal structure identification by electron diffraction analyses for the six bcc-derivative structures including A2, B2, B3, B32, $D0_3$ and $L2_1$ structures, which have no more than 16 atoms per unit cell, has been discussed by Dimiduk et al. [8]. Figure 3(a) is a bright field TEM image of a Ru-rich faceted precipitate enveloped by the γ matrix in the aged DS alloy UM-F13. The electron diffraction analyses indicate that the <111> zone-axis diffraction pattern of the present precipitate is identical for all six bcc-derivative structures, but the <001> zone-axis diffraction pattern (image not shown) suggests that the current

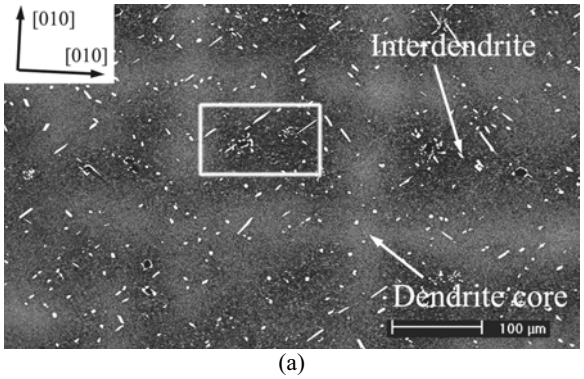


(a)

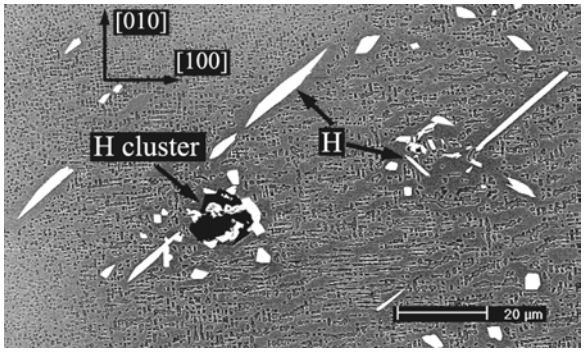


(b)

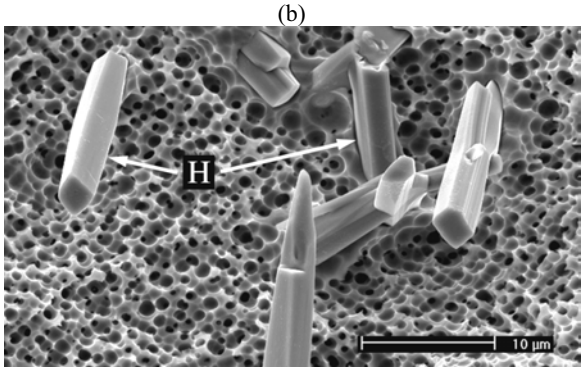


(c)

Figure 2. (a) a BSE image of the typical microstructure of a DS alloy UM-F13 after heat treatment at 1300°C/4 h + 1100°C/100 h, (b) a higher magnification image of the framed area in (a), (c) a SE image showing the morphology of H precipitates after an electrolytic extraction from the aged alloy UM-F13.

Table 4. Compositions of the H precipitates compared to dendritic microstructure in the experimental alloy UM-F13 (at. %).

| Material | Al | Co | Re | Ru | Ta | W | Ni |
|---|---|---|---|---|---|---|---|
| UM-F13 | 13.3 | 7.5 | 1.3 | 9.0 | 2.3 | 1.5 | 65.1 |
| H phase | 31.8 | 1.0 | 0.1 | 45.0 | 12.9 | 2.0 | 7.2 |
| Dendrite Core | 11.4 | 8.5 | 2.7 | 10.8 | 1.5 | 2.3 | 62.8 |
| Interdendritic | 14.4 | 7.5 | 0.8 | 8.1 | 2.2 | 1.1 | 65.9 |
| Eutectic | 16.1 | 5.7 | 0.2 | 7.2 | 4.7 | 0.2 | 65.9 |

phase is neither A2 nor B32 phase per the principle of kinematical forbidden reflections. The appearance of {111} and {311} superlattice diffraction intensities in the <011> zone-axis diffraction pattern, shown in Figure 3(b), eliminates the possibility of the B2 structure type. Further, the crystal point group of the B3 structure is known to be $\bar{4}3m$ while the $D0_3$ and $L2_1$ structures have the same m3m point group as well as the same space group. The technique of convergent beam electron diffraction (CBED) was used to determine the point group of the Ru-rich precipitate. Figure 3(c) is the CBED pattern of the <011> zone-axis taken from a precipitate, showing the 2mm diffraction symmetry. This distinguishes the m3m point group from the $\bar{4}3m$ structure. The CBED patterns of three low index zone-axes of the precipitates suggest the m3m crystal point group symmetry. These results restrict the precipitates to the Fm3m space group with either the $D0_3$ or the $L2_1$ structure type.

The $D0_3$ and $L2_1$ crystal structures are already shown in Figures 1(b) and (c). They can be distinguished from one another through structure factors or diffraction intensity differences, but electron diffraction intensity is affected by not only kinematical scattering, but also dynamical scattering associated with the specimen thickness. In practice, it is difficult to measure the precipitate composition and specimen thickness accurately by TEM, therefore the assurance of the computer-simulated relative electron diffraction intensity as a mean of identification of the crystal structure is still questionable. Since kinematical theory is more quantitative for X-ray diffraction due to its characteristic scattering behavior, the relative ratios of the theoretical X-ray diffraction intensities are needed to distinguish the $L2_1$ structure from the $D0_3$ structure. The experimental X-ray powder diffraction spectrum of the current precipitates extracted from the aged alloy UM-F13 suggested that the precipitates are the $L2_1$ type, rather than the $D0_3$ structure. The lattice parameter of this Heusler phase was calculated to be 0.6089 nm [9]. To further confirm the existence of this phase, a ternary alloy Ru25Al25Ta (atomic percent) was vacuum induction melted and annealed at 1100°C for 168 h, and milled into powder. The relative ratios of the experimental X-ray powder diffraction intensities of {111}, {311}, {331} superlattice reflections and {220} fundamental reflection were compared to the corresponding theoretically-calculated intensity differences [10]. The comparative X-ray results again indicated the matrix in the aged Ru25Al25Ta alloy was the $L2_1$ structure, not the $D0_3$ structure. To summarize, the phase identification by X-ray and electron diffraction analyses confirms that the current precipitates in the aged alloy UM-F13 are the $L2_1$ Heusler structure, $Ru_2AlTa$.

The selected area diffraction (SAD) pattern including both an H precipitate and the γ matrix spots can be indexed as shown in Figure 3(d). From this, the orientation relationship between the H and γ phases can be described as follows:

$$[001]_H // [0\bar{1}1]_\gamma \text{ and } (110)_H // (111)_\gamma .$$

This is the common Nishiyama-Wassermann relationship.

The B2 Phase RuAl

The B2 phase RuAl was first observed in both the as-cast and heat-treated multicomponent Ni-base superalloy UM-F16, which contains high levels of Ru (6.0 at.%/9.6 wt.%) and Cr (8.0 at.%/6.7 wt.%).

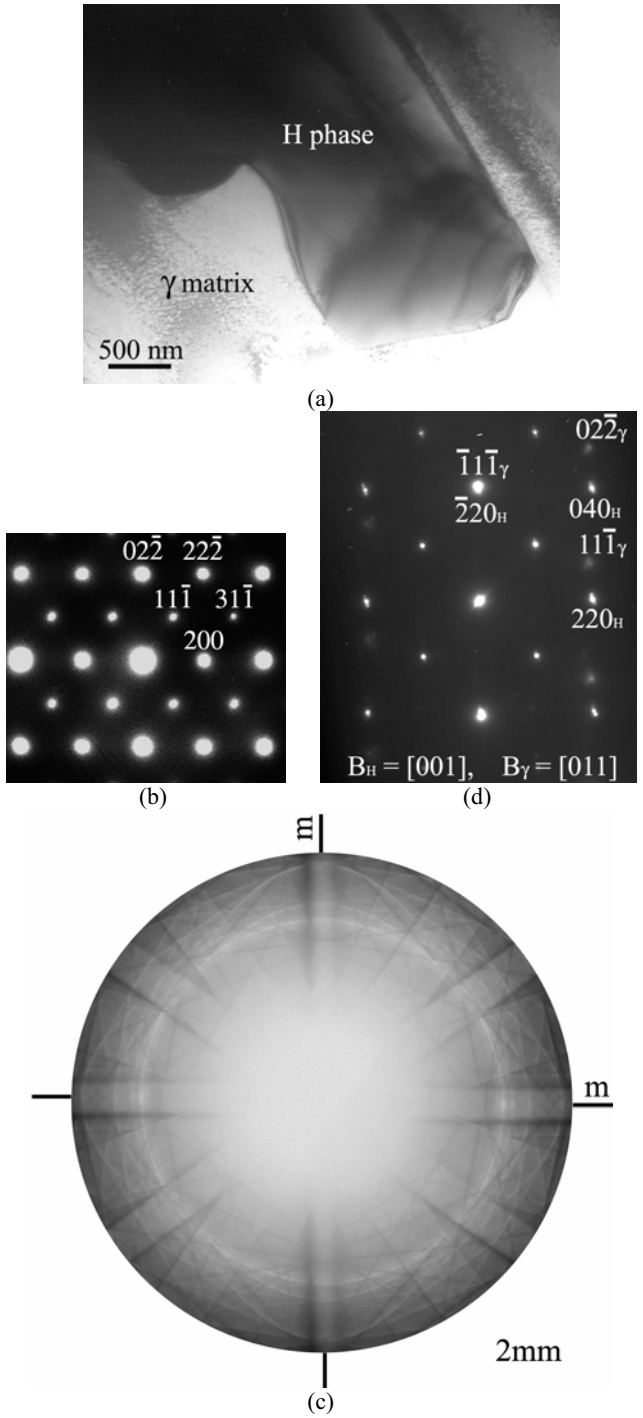


Figure 3. TEM diffraction analyses of the H precipitates from alloy UM-F13 after heat treatment at 1300°C/4 h + 1100°C/100 h, (a) a bright field image of the faceted H precipitate enveloped by the γ matrix, (b) <011> diffraction pattern of a H precipitate, (c) <011> CBED pattern showing 2mm whole pattern symmetry, (d) an indexed SAD pattern including both an H precipitate and the γ matrix spots.

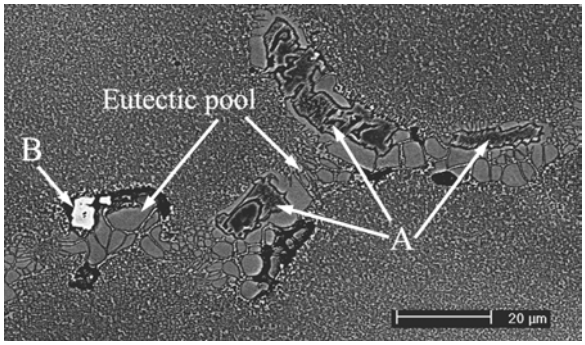


(a)

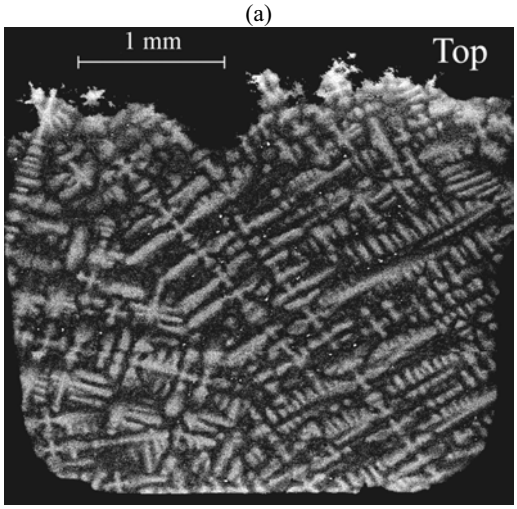


(b)

Figure 4. BSE images of the as-solidified alloy UM-F16 showing (a) two unusual Ru and Al-rich phases in the eutectic pools: NiAl-based β phase (dark gray, marked by A) and RuAl-based B2 phase (bright contrast, marked by B), (b) the distribution of the RuAl-based phase (bright contrast) taken from the DTA sample in the longitudinal section after testing.

marked by "A" and brightly contrasting phase marked by "B". The compositions measured by microprobe analyses (shown in Table 5) indicate that both phases are mainly enriched in Ru and Al, while higher levels of Ru in phase "B" appear to substitute for Ni compared to phase "A". This suggests that phase "B" is the B2-type RuAl-based solid solution, referring to the composition of RuAl in the Ni-Al-Ru ternary system [7]. Figure 4(b) is a BSE image of a cylindrical DTA sample in the longitudinal section after complete melting and re-solidification used to investigate the distribution of the RuAl-based particles. The very limited amounts of small, brightly-contrasting RuAl-based particles were present in the interdendritic regions and distributed uniformly from the bottom to the top of the sample. Further, microstructural observations at higher magnification indicated that no equiaxed grains or γ dendrites surrounded these particles. These features suggest that RuAl particles precipitated below the liquidus temperature, where the γ phase solidified first.

Figure 5(a) shows two bulk particles (marked by "A") with a serrated surface morphology enveloped by the γ' phase in a (γ + γ') eutectic pool of the as-solidified alloy UM-F16. They are the same phase as the "A" particles in Figure 4(a) and were frequently observed in the eutectic regions. Needle-like precipitates inside the particles were also observed within the particle "A". Figure 5(b) is a TEM bright field image of a Ru and Al-rich bulk phase, enveloped by the γ' phase in an eutectic region of alloy UM-F16. It contained these fine plate-like precipitates, which most likely developed during cooling. This is consistent with the SEM observation in Figure 5(a). The electron diffraction analyses indicate that this bulk phase is the B2 crystal structure, and is the NiAl-based β phase. Interestingly, RuAl-based and NiAl-based B2 phases co-existed as the separate phases in this as-cast alloy.

Table 5. Compositions of multiple Ru-rich phases existed in the experimental alloy UM-F16 (at. %).

| Material | Al | Co | Cr | Re | Ru | Ta | W | Ni |
|---|---|---|---|---|---|---|---|---|
| UM-F16 | 14.3 | 7.5 | 8.0 | 1.3 | 6.0 | 2.3 | 1.5 | 59.1 |
| A (NiAl)[a] | 33.6 | 3.9 | 6.4 | 0.2 | 17.3 | 1.7 | 0.3 | 36.7 |
| B (RuAl)[a] | 34.1 | 2.4 | 4.2 | 0.1 | 29.9 | 5.7 | 0.8 | 22.9 |
| Fmr Eut[b] | 27.8 | 4.3 | 4.2 | 0.2 | 11.1 | 2.4 | 0.6 | 49.3 |
| H phase[c] | 28.1 | 2.4 | 4.5 | 0.9 | 41.1 | 9.2 | 4.0 | 9.8 |
| RuAl[c] | 35.6 | 0.4 | 4.5 | 0.0 | 45.5 | 6.1 | 0.3 | 7.7 |
| δ phase[d] | 1.9 | 11.6 | 17.3 | 13.0 | 27.2 | 0.5 | 1.6 | 26.8 |

[a] as-cast condition;
[b] former eutectic regions after solution treatment at 1300°C/12h;
[c] using EDS in the SEM on extracted residues in the aged sample;
[d] using EDS in the TEM on the precipitates in the aged sample.

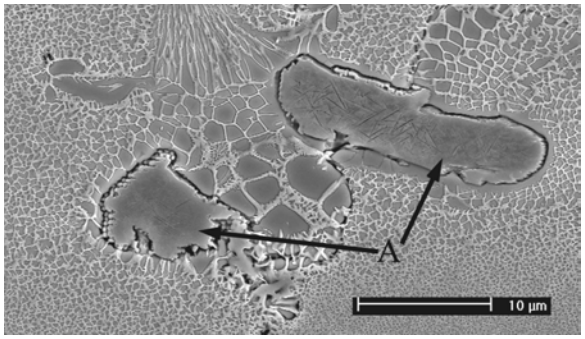


(a)

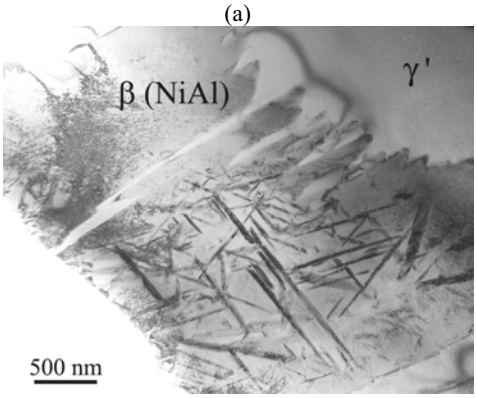


(b)

Figure 5. In the as-solidified alloy UM-F16, (a) a SE image showing two β(NiAl) bulk particles (marked by "A") enveloped by the γ' phase in an eutectic pool, (b) a TEM bright field image showing the bulk β phase contained fine plate-like precipitates.

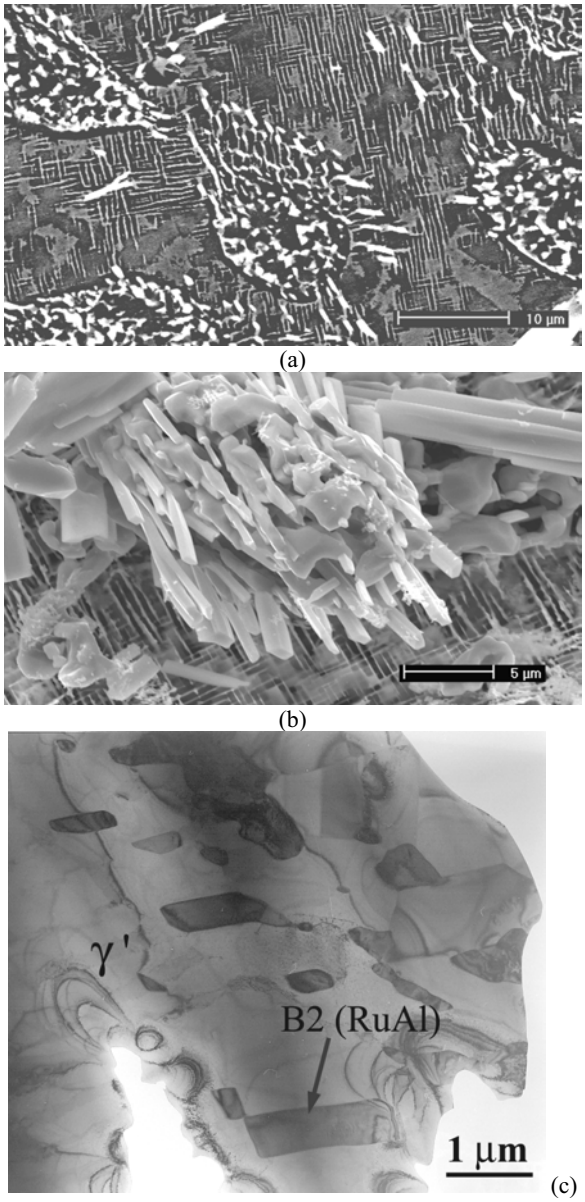


Figure 6. The former eutectic pools of alloy UM-F16 following annealing at 950°C for 1500h, (a) a BSE image showing the clusters of Ru-rich precipitates (white contrast), (b) the morphology of the precipitate cluster after an electrolytic extraction, (c) a TEM bright field image showing the precipitates inside a former eutectic pool.

After solution treatment at 1300°C/12h, significant amounts of the undissolved γ' phase existed in the former eutectic pools of alloy UM-F16. The average composition of the pools was measured by a microprobe and is listed in Table 5. Again, enrichment in Ru and Al was indicated. Figure 6(a) is a BSE image showing the clusters of brightly contrasting precipitates in the former eutectic regions after the solution-treated sample was aged at 950°C/1500h. Extracted from the same sample, the morphologies of the clustered precipitates are shown in Figure 6(b) to have faceted rod-like and blocky appearance or irregular plate-like shapes due to coarsening. Figure 6(c) is a TEM bright field image of the precipitates inside a former eutectic region. One faceted precipitate was selected for phase identification. The electron diffraction analyses indicated it was the B2 structure. The orientation relationship between the B2 precipitate and the surrounding γ' matrix was identified as:

$$[001]_{B2} // [0\,\bar{1}\,1]_{\gamma'} \text{ and } (110)_{B2} // (111)_{\gamma'}.$$

Again, this is the Nishiyama-Wassermann orientation relationship between the fcc (γ') and bcc-derivative (B2) structures.

Figure 7(a) is a BSE image of the typical microstructure in the former dendritic region of alloy UM-F16 aged at 950°C for 1500h. Besides the γ and γ' phases, it consisted of brightly contrasting plate-like precipitates marked by "A" and fine needle-like precipitates with the basket weave morphology labeled "B".

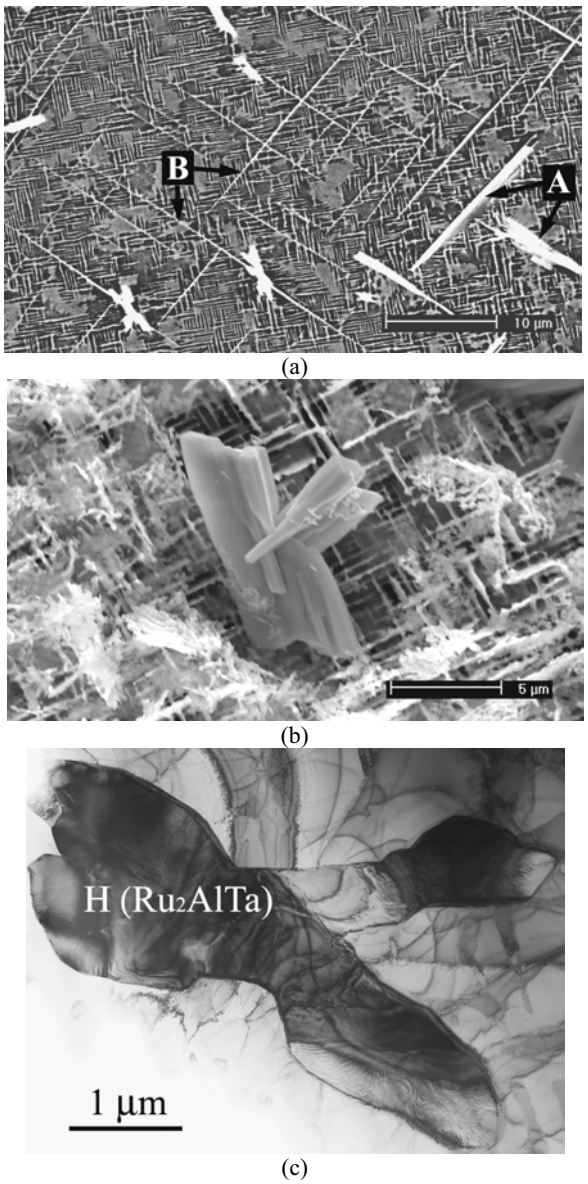


Figure 7. The former dendritic region of alloy UM-F16 following annealing at 950°C for 1500h, (a) a BSE image showing the typical microstructure, (b) the morphology of the precipitates after an electrolytic extraction, (c) a TEM bright field image of two H precipitates intersecting each other.

The needle-like precipitates will be identified in the following section. Figure 7(b) shows the morphology of a larger faceted precipitate located in the former dendritic region, which is similar to precipitates labeled "A" in Figure 7(a). Figure 7(c) is a TEM bright field image of two adjacent precipitates in the former dendritic region. The precipitates were identified as the $L2_1$ Heusler structure by electron diffraction analyses. The microstructure and morphologies of these precipitates in the aged alloy UM-F16 are consistent with both SEM and TEM observations.

Since the precipitates in this aged alloy were too fine to be analyzed quantitatively, semi-quantitative analyses with EDS in the SEM were conducted on the extracted precipitates. The compositions of the B2 and H phases are also listed in Table 5 and again they were enriched in Ru, Al and Ta. The observed B2 and H precipitates possess structures based on RuAl and $Ru_2AlTa$ phases, respectively. The chemical analyses also suggest that 1) both B2 and H phases precipitated in both dendritic and interdendritic regions; 2) there were no significant composition differences between the dendritic and interdendritic regions for the B2 and H precipitates, respectively.

The Re(Ru)-rich hcp δ phase

The hcp δ–Re phase has been reported in as-cast and heat treated Ni-Al-Re ternary alloys [11, 12]. The binary Re-Ru system is an isomorphous system, showing the complete Re-Ru solubility in the solid state [4]. Thus, it is expected that the hcp δ–Re(Ru) phase might exist in both as-cast and heat-treated Ru-containing multicomponent Ni-base alloy systems.

Figure 8(a) is a BSE image, showing the typical as-solidified microstructure of DS alloy UM-F3 sectioned normal to the growth direction. It consisted of misoriented γ dendrites and δ particles (bright contrast) located inside the interdendritic regions. The interdendritic microstructure is shown in Figure 8(b) at higher magnification and the brightly contrasting δ particles are associated with porosity and a large volume fraction of γ' in the interdendritic region. Figure 8(c) shows a δ particle residing in an as-cast bulk sample after phase extraction. It clearly possesses a dendritic morphology, but the growth has been apparently restricted by the surrounding matrix, resulting in a loss of the six-fold dendritic morphology [5]. Further, δ particles were distributed homogeneously along the growth direction. This suggests that the δ particles developed below the liquidus temperature of the γ primary phase and did not act as grain nucleation sites during the solidification. Therefore, the solidification sequence in this alloy is suggested as follows:

$$L \rightarrow L_1 + \gamma \rightarrow L_2 + \delta + \gamma \rightarrow (\gamma + \gamma')_{eutectic} + \delta + \gamma \ .$$

Finer δ precipitates were observed in alloy UM-F3 after solution treatment at 1300°C for 4h and after aging treatment at 1150°C for 50h, respectively. They were preferentially located in the previous dendritic regions [5]. Figure 9(a) is a BSE image, showing the typical microstructure of another aged alloy UM-F14 after 1300°C/4h followed by 1100°C/100h. It consists of the γ phase (light gray), γ' precipitates (dark gray) in the γ phase and a large volume fraction of δ precipitates (bright contrast) enveloped by the γ' phase. Figure 9(b) shows the morphology of the δ precipitates left in a bulk sample after phase extraction. They appeared to be feather-like or possess irregular plate-like shapes.

The average compositions of the δ precipitates in the Cr-free alloys UM-F3 and UM-F14 were measured by a microprobe and are listed in Table 6. Compared to the nominal alloy compositions, the δ phase was significantly enriched in Re and Ru, but strongly depleted in Al and Ta. X-ray diffraction analyses of these extracted Re(Ru)-rich precipitates in both as-cast and aged conditions revealed that they were the hcp crystal structure, which was further confirmed by electron diffraction analyses. The orientation relationship between the δ phase and the surrounding γ' phase was identified as:

$$[11\bar{2}0]_\delta // [01\bar{1}]_{\gamma'} \text{ and } (0001)_\delta // (111)_{\gamma'} \ .$$

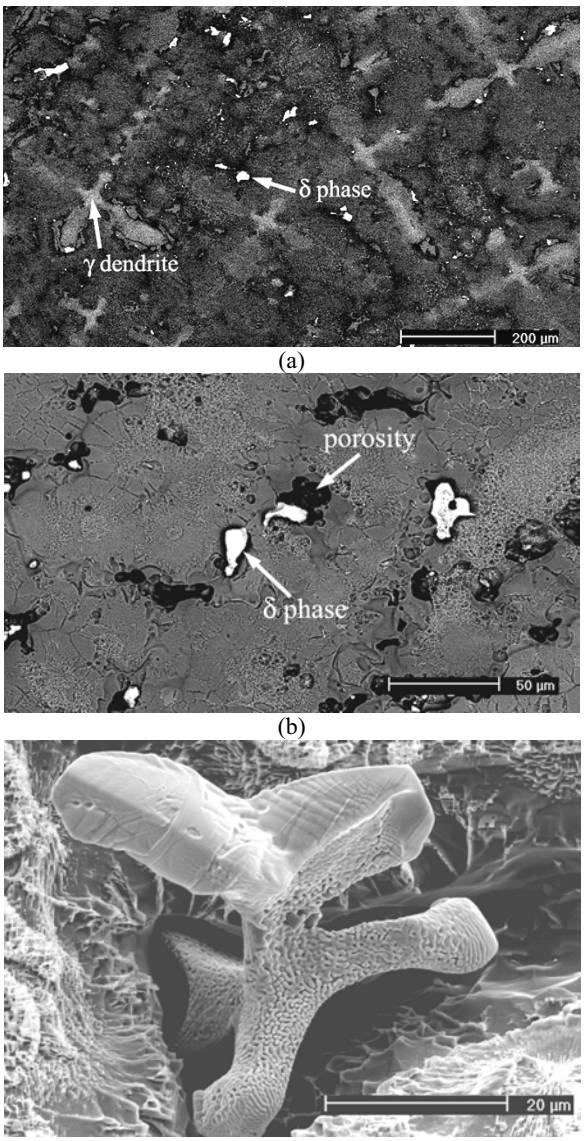


Figure 8. As-solidified alloy UM-F3 after DS processing, (a) a BSE image showing the typical microstructure, (b) a high magnification BSE image showing the δ phase associated with porosities located in the eutectic regions, (c) a SE image exhibiting the morphology of a δ dendrite residing in a bulk sample after phase extraction.

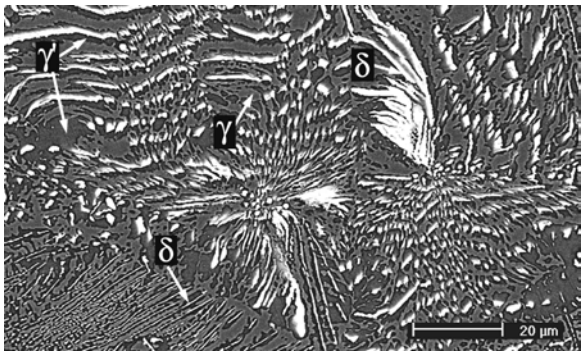


(a)

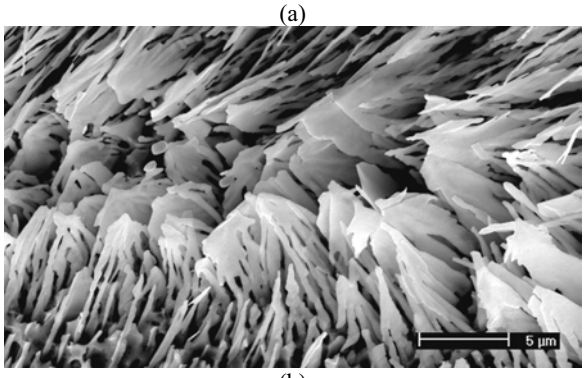


(b)

Figure 9. The aged alloy UM-F14 after 1300°C/4h followed by 1100°C/100h heat treatment, (a) a BSE image showing the typical microstructure, (b) a SE image showing the morphology of the δ precipitates left in a bulk sample after phase extraction.

Table 6. Compositions of the Re(Ru)-rich δ phase measured by microprobe analysis in alloys UM-F3 and UM-F14 (at.%).

| Materials | Al | Co | Re | Ru | Ta | W | Ni |
|---|---|---|---|---|---|---|---|
| UM-F3 | 18.4 | 7.5 | 1.8 | 2.5 | 2.5 | 1.5 | 65.8 |
| UM-F14 | 14.3 | 7.5 | 2.5 | 6.0 | 2.3 | 1.5 | 65.9 |
| δ (UM-F3)[a] | 0.5 | 9.8 | 48.1 | 14.8 | 0.4 | 5.2 | 21.2 |
| δ (UM-F3)[b] | 0.1 | 7.0 | 56.7 | 17.2 | 0.1 | 3.4 | 15.5 |
| δ (UM-F14)[b] | 1.0 | 4.8 | 36.5 | 31.3 | 0.4 | 3.1 | 22.9 |

[a] as-cast condition, [b] aged condition.

The lattice parameters of the δ phase measured from X-ray power diffraction spectra are given in Table 1 along with those of the H ($Ru_2AlTa$) and B2 (RuAl) phases. Detailed characterization of the Re(Ru)-rich δ phase (containing no Cr) has been reported elsewhere [5, 13].

In the previous section, the needle-like precipitates with the basket weave morphology were marked by "B" and are shown in Figure 7(a). They were preferentially located in the previous dendritic regions of the aged alloy UM-F16. Figure 10(a) is a TEM bright field image of the aged alloy UM-F16, exhibiting a microstructure similar to that observed by SEM. The precipitates were further identified as the plate-like by tilting. The average composition of these precipitates was measured using standardless EDS in the TEM and is given in Table 5 as labeled "δ phase". It indicated that Re, Ru and Cr were enriched by the factors of 10, 4.5 and 2.2 times, respectively, compared to the nominal alloy composition. Although the morphology and composition of these planar needle-like precipitates are similar to those of TCP phases [14, 15], systematic electron diffraction analyses consistently identified them as the hexagonal structure of the Ru(Re)-rich δ phase. Figure 10(b) shows an indexed SAD pattern including diffraction spots from both a δ precipitate and the γ' matrix, which present relatively weak and strong diffraction intensities, respectively. The orientation relationship between them is the same as one described in the last paragraph.

## Discussion

Modern single crystal superalloys have quite complex alloy compositions and contain more than ten alloying elements. Such complex multicomponent Ni-base alloy systems are often thermodynamically unstable with the respect to the precipitation of phases during long term thermal exposures. Many secondary phases beyond the γ and γ' phases are possible and their presence is a strong function of segregation, thermal history and alloy chemistry. In this study, a broad range of Ru additions (2.5-9 at.%/4-14 wt.%) were introduced into model single crystal alloys. Such high levels of Ru would be expected to influence the thermodynamics of these complex alloy systems. Three phases not previously observed in multicomponent superalloys associated with Ru additions were identified in the present work: a $Ru_2AlTa$-based intermetallic phase ($L2_1$ Heusler structure), a RuAl-based intermetallic phase (B2 structure) and a Re(Ru)-based solid solution (δ phase, hcp structure). Table 7 summarizes the findings

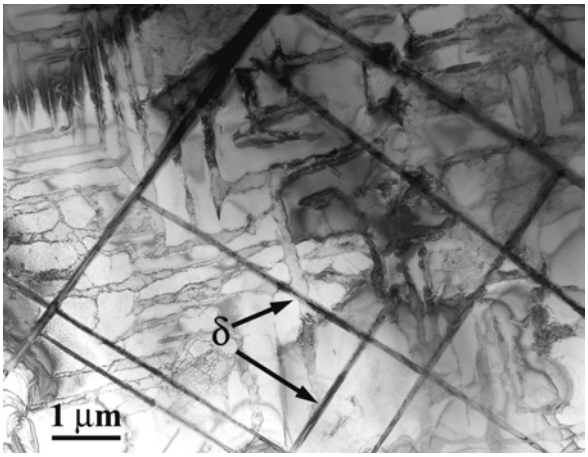


(a)

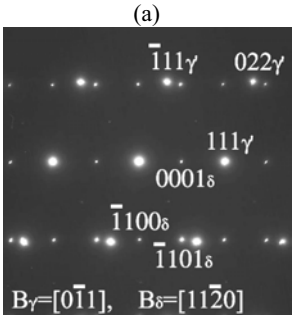


(b)

Figure 10. The former dendritic region of alloy UM-F16 following annealing at 950°C for 1500h, (a) a TEM bright field image of the planar-like δ precipitates with the basket weave morphology, (b) an indexed SAD pattern including both a δ precipitate and the γ' matrix spots.

Table 7. Ru-rich new phases present (marked by "√") in the as-cast and/or aged investigated superalloys.

| | UM-F3 | | UM-F9 | | UM-F13 | | UM-F14 | | UM-F16 | |
|---|---|---|---|---|---|---|---|---|---|---|
| | Cast | Aged | Cast | Aged | Cast | Aged | Cast | Aged | Cast | Aged |
| H phase | | | | | | √ | | | | √ |
| B2 phase | | | | | | | | | √ | √ |
| δ phase | √ | √ | | | | | √ | √ | | √ |

in terms of the alloys in which these phases precipitated. The existence of these phases is not very surprising since the same type phases, albeit with different chemistries exist in the Ni-X binary, Ni-Al-X ternary or Ni-based multicomponent systems. Among these are the B2 phase NiAl(β), the H phase $Ni_2AlTa$ and $Ni_2AlNb$ as well as hcp phase δ-(Re) and (Ru) in the Ni-Al-Re and Ni-Al-Ru ternary systems, respectively.

The $Ru_2AlTa$ H phase was first discovered here as an equilibrium phase co-existing with the γ and γ' phases at 1100°C in alloy UM-F13 and was stabilized by high levels of Ru additions. This phase was also confirmed to exist in the ternary system as Ru25Al25Ta at 1100°C. Based on this finding, the intermetallic compound $Ru_2AlTa$ has been further investigated in the bulk form and has exceptional resistance to deformation at high temperature [16]. Although the RuAl B2 phase exists in the Ru-Al binary and Ni-Al-Ru systems, research on the role of B2 phase Ru(Al, Ta) in multicomponent Ni-base superalloys is limited. The B2 phase RuAl was found to co-exist with $Ru_2AlTa$-based H precipitates in alloy UM-F16 aged at 950°C/1500h. The $L2_1$ $Ru_2AlTa$ is a highly ordered intermetallic phase derived from the ordered B2 phases RuAl and RuTa. This Heusler lattice has a large unit cell composed of 8 RuAl or RuTa unit cells, in which Al and Ta atoms occupy ordered sites on one sublattice (Figures 1(a) and (b)). The observed B2 RuAl precipitates may be metastable if the highly ordered Heusler phase $Ru_2AlTa$ is stable at lower temperature (950°C). Also, faint intensities appeared at the locations of {111} and {311} H superlattice spots in the <011> zone-axis diffraction pattern of some B2 precipitates in the current study, suggesting the development of further ordering. Previously studied ternary Ni-17Al-xRe alloys with more than 2 at.% Re are in the (γ + γ'+ δ) three-phase equilibrium region at 1040°C [12], while Ru additions up to about 8 at.% are still in (γ + γ') two-phase field at 1000°C in the Ni-17Al-xRu ternary system [7]. No (γ + γ' + (Ru)) three-phase field exists at 1000-1250°C in the Ni-Al-Ru ternary system. The present work shows that alloy UM-F14 containing Re (2.5 at.%), Ru (6 at.%) and Al + Ta (16.6 at.%) is in a (γ + γ'+ δ) three-phase field at 1100°C. This suggests that the characteristics of multicomponent Ni-base systems (containing Ru and Re) thermodynamically resemble the Ni-Al-Re ternary system more than the Ni-Al-Ru ternary system. It is interesting to note that no significant secondary phases precipitated at 950°C/1500h in the baseline alloy UM-F9 while three Ru-rich phases (H, B2 and δ) all appeared in alloy UM-F16 with the same heat treatment condition. The only chemistry difference between two alloys is the Cr addition in alloy UM-F16. This suggests that Cr additions strongly affect the thermodynamics of this multicomponent system and promote formation of these phases. It also should be noted that the composition of the δ phase in alloy UM-F16 was also enriched in Cr. This suggests that Cr substituted for Re compared to the δ phase in Cr-free alloy UM-F14.

The current study has shown that the precipitation of H and B2 phases occurred uniformly throughout the dendritic structure except for some clustering in the former eutectic pools, conversely, the δ phase preferentially precipitated in the dendritic regions. The location preference of precipitation is expected to be influenced by the elemental segregation during solidification as well as residual chemical inhomogeneity after solution treatment. Chemical analyses suggest that Ru and Al as well as Ta strongly partitioned to the H and B2 phases while the δ phase was strongly enriched in Re and Ru as well as Cr. The microprobe results given in Table 4 are a typical example for the larger series of Ru-containing superalloys in this investigation, and show the segregation behavior of individual constituents similar to the as-cast alloy UM-F13, including: 1) Re and W strongly segregated to the dendrite cores, 2) Ta and Al significantly partitioned to the interdendritic regions with the strong enrichment of Ta in the eutectic pools and 3) Ru preferentially partitioned to the dendrite cores with less pronounced segregation behavior. This is also consistent with the segregation mapping analyses in another study [17]. For example, the ranges of the distribution coefficients (k) for Ru, Re, Ta and Al assessed from the modified Scheil analyses are 1.07-1.15, 1.51-1.81, 0.67-0.76 and 0.83-0.91 respectively, in a series of Ru-containing superalloys. Less segregation is indicated by a k value close to the unity. Recent studies on inter-diffusion of elements in pure nickel at 900-1300°C generally show the interdiffusion coefficients in an ascending order: Re < Ru < W < Ta [18, 19]. The residual chemical inhomogeneity depends on not only the elemental diffusion, but also the elemental solidification segregation. Strong segregation and slow diffusion of elements result in heavy residual inhomogeneity after solution treatment, of Re, W and Ta in contrast to Ru, which has less pronounced segregation. Therefore, with respect to the phase compositions, it is understandable that the H and B2 phase precipitated fairly uniformly in both dendritic and interdendritic regions due to homogenous distribution of Ru. However, the residual enrichment of Ta in the former eutectic pools resulted in some clustering of H and B2 precipitates. The location preference of the δ phase was strongly influenced by the Re profile, which has the strongest residual inhomogeneity in the dendritic regions. Similar features have been observed in the precipitation of TCP phases [14].

It is interesting to note that RuAl-based and NiAl-based B2 phases co-existed as the separate phases in the as-cast alloy UM-F16 (Figure 4(a)). Chakravorty and West investigated the Ni-Al-Ru ternary phase diagram and reported a miscibility gap between RuAl-based and NiAl-based phases, resulting in a region consisting of two distinct B2 compounds [7]. Later, Horner et al. suggested that the apparent two-phase microstructure could be interpreted as a cored structure instead of two distinct B2 phases, due to the indistinct boundary between them [20]. Recent X-ray studies on ball-milled materials and first principle type calculations supported the observations by Horner et al., and have suggested that there was not a miscibility gap, but a single continuous B2 phase field between RuAl and NiAl [21, 22]. However, the current observations clearly indicate that RuAl and NiAl can be two distinct separate B2 phases in the

multicomponent Ni-base alloy in the as-solidified state. Further work is required to fully understand the equilibrium conditions under which these B2 phases appear in superalloys.

The existence of new Ru-rich phases indicates a limit to the useful levels of Ru additions in this class of superalloys. The phases observed in this study are not likely to improve creep properties. The present work suggests that the levels of Ru, Re, Ta and Cr additions have the most significant influence on the formation of these phases, so these elements must be balanced if Ru additions are pursued for the next generation of single crystal alloys.

## Conclusions

1. Three new phases not previously observed in multicomponent superalloys have been identified in the current work: a $Ru_2AlTa$-based intermetallic phase ($L2_1$ Heusler structure), a RuAl-based intermetallic phase (B2 structure) and a Re(Ru)-based solid solution (δ phase, hcp structure).

2. The H and δ phases are promoted by high levels of Ru and Re additions, respectively, and they are stable at 1100°C. With annealing at 950°C/1500h, the three new phases co-existed in a Ru-containing alloy with Cr additions, indicating that Cr plays a special role in the formation of these Ru-rich phases.

3. In the aged condition, the δ phase preferentially precipitated in the former dendritic regions while the H and B2 phases precipitated fairly uniformly in both dendritic and inter-dendritic regions with some clustering of these precipitates located only in the previous eutectic pools. These features can be explained by the elemental segregation behavior and the residual chemical inhomogeneity of Ru, Re and Ta.

4. The H, B2 and δ phases can be distinguished by their compositions. The H and B2 phases were strongly enriched in Ru, Al and Ta, while heavily depleted in Re and Co. In the δ phase, Ru and Cr substituted for Re with a trace of Al and Ta.

5. These new phases all exhibit characteristic morphologies and orientation relationships with γ or γ' phases.

## Acknowledgments

The authors are grateful to C. Henderson, A. Elliot, C. Okafor and C. Torbet for their experimental assistance in this study. Useful technical discussions with M. De Graef, M. Konter and P. Holmes are greatly appreciated. The financial support provided by Alstom Power, Ltd. is gratefully acknowledged.

## References

1. W.S. Walston, "Turbine Airfoil Material Issues for Aircraft Engines", *Advanced Materials and Processes for Gas Turbines*, eds. by G. Fuchs et al. (Warrendale, PA: The Minerals, Metals and Materials Society, 2003) 35-41.
2. K.S. O'Hara, W.S. Walston, E.W. Ross, R. Darolia, "Ni-base superalloy and article", *U. S. Patent*, No. 5,482,789, 1996.
3. P. Caron, "High γ' Solvus New Generation Nickel-based Superalloys for Single Crystal Turbine Blade Applications", *Superalloys 2000*, eds. T. M. Pollock et al. (Warrendale, PA: The Minerals, Metals and Materials Society, 2000) 737-746.
4. T.B. Massalski et al., eds., *Binary Alloy Phase Diagrams, 2nd edition*, (Materials Park, OH: ASM International, 1990).
5. Q. Feng, T.K. Nandy, S. Tin, T.M. Pollock, "Solidification of High-refractory Ruthenium-containing Superalloys", *Acta Mater.*, 51 (2003) 269-284.
6. J.X. Zhang, T. Murakumo, Y. Koizumi, T. Kobayashi, H. Harada, S. Masaki Jr., "Interfacial Dislocation Networks Strengthening a Fourth-Generation Single-Crystal TMS-138 Superalloy", Metall. Mater. Trans. A, 33 (2002) 3741-46.
7. S. Chakravorty, D.R.F. West, "The Constitution of the Ni-Al-Ru System", *Journal of Materials Science*, 21 (1986) 2721-2730.
8. D.M. Dimiduk, M.G. Mendiratta, D. Banerjee, H.A. Lipsitt, "A Structural Study of Ordered Precipitates in an Ordered Matrix within the Fe-Al-Nb System", *Acta Metall.*, 36 (11) (1988) 2947-2958.
9. Q. Feng, T.K. Nandy, T.M. Pollock, "Observation of a Ru-rich Heusler Phase in a Multicomponent Ni-Base Superalloy", *Scripta Mater.*, 50 (2004) 849-854.
10. M. De Graef, private communication with authors, Carnegie Mellon University, February, 2003.
11. L.A. Cornish, M.J. Witcomb, "A Metallographic Study of the Al–Ni–Re Phase Diagram", *J. Alloys Compounds*, 291 (1999) 145-166.
12. S. Miyazaki, H. Murata, M. Morinaga, "Site Occupancy of Re Atoms in $Ni_3Al(\gamma')$ and γ–γ' Phase-Equilibria in Ni-Al-Re Ternary Alloys", *Tetsu-To-Hagane*, 80 (2) (1994) 161.
13. Q. Feng, T.K. Nandy, T.M. Pollock, "The Re(Ru)-rich δ phase in Ru-containing Superalloys", *Mater. Sci. Engin. A*, 373 (2004) 239-249.
14. C.M.F. Rae, M.S.A. Karunaratne, C.J. Small, R.W. Broomfield, C.N. Jones, R.C. Reed, "Topologically Close-packed Phases in an Experimental Rhenium-containing Single Crystal Superalloys", *Superalloys 2000*, eds. T. M. Pollock et al. (Warrendale, PA: The Minerals, Metals and Materials Society, 2000) 767-776.
15. C.M.F. Rae, R.C. Reed, "The Precipitation of Topologically Close-packed Phases in Rhenium-Containing Superalloys", *Acta Mater.*, 49 (2001) 4113-4125.
16. Q. Feng, T.K. Nandy, B. Tryon, T.M. Pollock, "Deformation of Ru-Al-Ta Ternary Alloys", *Intermetallics*, (2004), in press.
17. Q. Feng, L.J. Rowland, T.M. Pollock, "Solidification Segregation in Ru-containing Nickel-base Superalloys", in preparation for submission to *Metall. Mater. Trans. A.*
18. M.S.A. Karunaratne, R.C. Reed, "Interdiffusion of the Platinum-group Metals in Nickel at Elevated Temperature", *Acta Mater.*, 51 (2003) 2905-2919.
19. M.S.A. Karunaratne, P. Carter, R.C. Reed, "Interdifussion in the Face-centered Cubic Phase of the Ni-Re, Ni-Ta and Ni-W Systems between 900 and 1300°C", *Mater. Sci. Engin. A*, 281 (2000) 229-233.
20. I.J. Horner, N.Hall, L.A. Cornish, M.J. Witcomb, M.B. Cortie, T.D. Boniface, "An Investigation of the B2 Phase between AlRu and AlNi in the Al-Ni-Ru Ternary system", *J. Alloys Compound*, 264 (1998) 173-179.
21. K.W. Liu, F. Mucklich, W. Pitschke, R. Birringer, K. Wetzig, "Formation of Nanocrystalline B2-structured (Ru,Ni)Al in the Ternary Ru–Al–Ni System by Mechanical Alloying and its Thermal Stability", *Mater. Sci. Eng. A*, 313 (2001) 187-197.
22. P. Gargano, H. Mosca, G. Bozzolo, R.D. Noebe, "Atomistic Modeling of RuAl and (RuNi)Al Alloys", *Scripta Mater.*, 48 (2003) 695-700.